GEOLOGICA CARPATHICA, DECEMBER 2022, 73, 6, 561–577 https://doi.org/10.31577/GeolCarp.73.6.4

Review article

Post-Cretaceous–Paleogene slumping in the Subsilesian Unit of the Outer Western Carpathians: Biostratigraphic, sedimentary and magnetic records from the Bystřice section

MIROSLAV BUBÍK[1,✉], TIIU ELBRA[2], JURAJ FRANCŮ[1], ŠIMON KDÝR[2,3], PETR SCHNABL[2] and LILIAN ŠVÁBENICKÁ[4]

[1]Czech Geological Survey, Leitnerova 22, 60200 Brno, Czech Republic; ✉miroslav.bubik@geology.cz
[2]Institute of Geology of the Czech Academy of Sciences, Rozvojová 269, 16500 Praha, Czech Republic; elbra@gli.cas.cz, schnabl@gli.cas.cz, kdyr@gli.cas.cz
[3]Institute of Geochemistry, Mineralogy and Mineral Resources, Faculty of Science, Charles University, Albertov 6, 12843 Praha, Czech Republic; kdyr@natur.cuni.cz
[4]Czech Geological Survey, Klárov 3, 11821 Praha, Czech Republic; lilian.svabenicka@geology.cz

(Manuscript received July 1, 2022; accepted in revised form November 16, 2022; Associate Editor: Jozef Michalík)

Abstract. The Bystřice section, which was previously interpreted as the continuous Cretaceous–Paleogene transition, has been newly studied using biostratigraphy (planktonic foraminifers, calcareous nannofossils), magnetic properties, and geochemistry. Biostratigraphy has confirmed the presence of the upper Maastrichtian (UC20d^{TP} nannozone; *Abathomphalus mayaroensis* foraminifer zone) and Selandian (NP5–NP7 nannozones; P3b–P4b foraminifer zones). Moreover, the Danian is completely absent. Strong remagnetisation of the rocks did not enable magnetostratigraphy of the section. The magnetic fabric indicates tectonic disturbance of the section. The studied strata consist predominantly of paraconglomerates, which are interpreted as slumps. The slumps contain pebbles and blocks of diverse exotic rocks, intraclasts, and reworked carbonate concretions enclosed within a marly matrix. A few thick paraconglomerate bodies are separated by bedded grey silty marls, sequences of medium-rhythmic sandstone turbidites, and conglomerate. Frequent slump folds indicate synsedimentary deformation. Submarine landslides are manifested by folded and thrusted sandstone beds, breccia of partly-lithified sandstones, and characteristic failure planes. In the lower part of the section, marls and paraconglomerates with Maastrichtian microfossils are interbedded with marls containing Selandian microfossils. It is most likely that the whole of the studied sequence was deposited during the Selandian, and that Maastrichtian marls and paraconglomerates represent submarine mass flows. The deposition took place on the basin slope in the bathyal zone. The geochemical proxy parameters indicate more reducing setting, higher input of terrestrial phytodetrite, as well as higher surface-water temperatures in the Maastrichtian, which is confirmed also by occurrences of low-latitude nannoplankton. The Selandian sediments contain a higher share of aquatic organic matter. The pristane/phytane ratio indicates an oxygenated water column, and carbonate $\delta^{13}C$ and $\delta^{18}O$ isotopes point to lower surface-water temperatures.

Keywords: Western Carpathians, Frýdek Formation, Maastrichtian, Paleocene, planktonic foraminifers, calcareous nannofossils, sedimentology

Introduction

A cataclysmic event at the end of the Cretaceous period continues to attract both scientists and the public due to global extinction, which is affecting a large number of species. In fact, evidence of a cataclysmic event and global extinction has already been clearly proven by robust data from many dozens of geological archives worldwide. Nonetheless, discussions continue, whether the abrupt changes and consequent extinction were triggered by the impact of an extra-terrestrial body or enormous volcanic activity in the Deccan Plateau (Claeys et al. 2002; Kiessling & Baron-Szabo 2004; Keller et al. 2016; Petersen et al. 2016). Ongoing research on new sites may shed more light on this problem.

Shallow marine sequences are often incomplete because of erosion or non-sedimentation at the Cretaceous–Paleogene (K–Pg) boundary. Open marine facies are more suitable from this point of view. The Western Carpathians offer the opportunity to study the K–Pg transition in most of their nappe units. One of them is the Subsilesian Unit with a record of Cretaceous and Paleogene hemipelagic sediments.

Hanzlíková & Švábenická (1983) described the K–Pg transition at the Bystřice section in the facies of the slope marls and pebbly mudstones within the Frýdek Formation of the Subsilesian Unit. Eva Hanzlíková also prepared a distribution chart of foraminifers for the section that documents the K–Pg transition (this is an unpublished printout for field-trip participants). Since then, however, the section has not been studied in detail.

The microfossil record, including planktonic foraminifers and calcareous nannofossils, is generally good in the grey slope marls of the Frýdek Formation. The Bystřice section was therefore considered to be promising for bio- and magnetostratigraphic investigations of the K–Pg boundary events. However, preliminary biostratigraphic results clearly proved that sediments with Paleocene microfossils are interbedded with sediments containing Maastrichtian microfossils several times over. Moreover, the Paleocene microfossils are of Selandian age, while the Danian ones are completely absent. Thus, this poses several questions about the sedimentary history of the studied section.

This paper provides a possible interpretation of the stratigraphical gap in the Lower Paleocene, as well as of the stratigraphic repetition of the Paleocene in the section as a result either of tectonic duplication or mass flows of older sediments.

Geological setting

The area studied is situated in the Outer Western Carpathians, which is the most external zone of the Carpathian Mountain chain, a part of the Alpine–Carpathian–Dinaridic orogenic system. The Outer Carpathians are a structurally-complex area consisting of folded and thrusted uppermost Jurassic to Lower Miocene strata. In the territory of the Czech Republic, the Outer Western Carpathians consist of two groups of nappes: the Outer Group of Nappes (divided from the lowest to the highest into the Ždánice–Subsilesian, Silesian, and Foremagura nappes) and the Magura Group of Nappes (Fig. 1). The entire nappe allochthon is thrusted more than 60 km over the Miocene sediments of the Carpathian Foredeep as a result of a major tectonic event in the Middle Miocene (Picha et al. 2006).

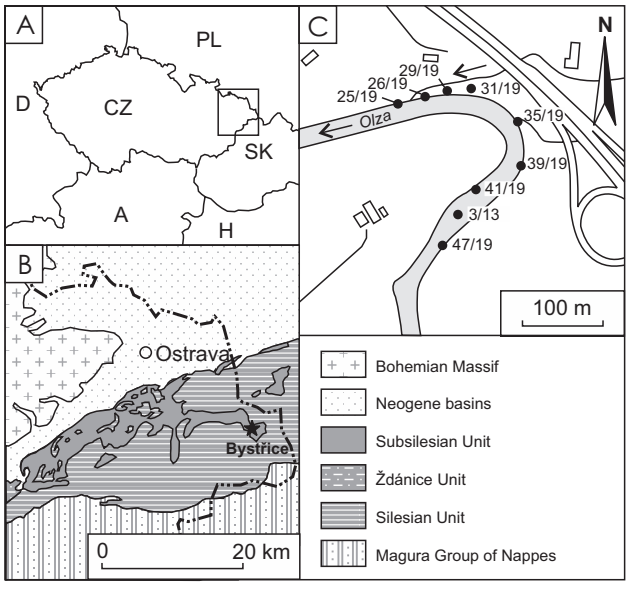

Fig. 1. Situation of the Bystřice section on the tectonic map of area indicated by asterisk (**A**, **B**) and the topographic situation of the section with the position of selected micropaleontological samples indicated by dots (**C**).

The Subsilesian Nappe consists of Upper Cretaceous to Lower Miocene hemipelagic and flysch sediments deposited in the Silesian Basin (Menčík et al. 1983; Picha et al. 2006), which represent marine sediments of the continental slope and ridge. The nappe is subdivided into four lithostratigraphic units (from the oldest): the Frýdek, Frýdlant, Menilite, and Ženklava formations (Eliáš 1998; Bubík et al. 2016).

The dominant lithology of the Frýdek Formation consists of grey silty marls that locally include thick sequences of grey calcareous turbiditic sandstones and bodies of paraconglomerates with blocks of exotic rocks (Menčík et al. 1983; Stráník 2021). Such lithology can also be seen in the studied section in Bystřice (Fig. 2).

Methods

The studied section is situated in the right cut of the Olše River along the large meander (Fig. 2). The GPS position of the lowest bed is 49°38’23.9”N, 18°42’17.1”E; the highest bed is 49°38’18.1”N, 18°42’19.0”E. A nearly continuous outcrop exposes steep to medium-tilted beds with a general dip to the southeast.

Nannofossil samples were crushed into powder and poured into distilled water. Obtained suspension was placed on a glass slide, dried, and mounted in Canada Balsam. The slides were observed under a Nikon Microphot-FXA transmitting light microscope with an oil immersion objective of ×100 magnification. Taxonomic concepts follow Burnett (1998), Varol (1998), and the Nannotax website (Young et al. 2018a). Biostratigraphic data were interpreted with reference to the nannofossil zonations of Martini (1971) and Burnett (1998). Semiquantitative analysis follows methodology of Bown & Young (1998) and Burnett & Whitham (1999).

Foraminifer samples were soaked in a warm solution of sodium carbonate and washed on a 0.063 mm sieve under tap water. Foraminifers were manually picked and observed under a Zeiss microscope. Important taxa were documented by SEM electrographs using the electron microscope JEOL JSM-6380LV. Planktonic foraminifer taxonomy and biostratigraphy follow the concept from the Microtax website (Young et al. 2018b). The nannofossil slides are currently being stored at the Czech Geological Survey, Prague, while the foraminifers and foraminifer residues are being stored at the Czech Geological Survey in Brno.

In addition to the biostratigraphic research, the Bystřice section was also studied for rock- and paleomagnetism. Magnetic susceptibility (MS) of the section was first measured *in situ* in the field where possible, every 1 metre in distance, using a portable Terraplus Kappameter KT-10. Each spot was measured at least twice and averages were calculated. Obtained MS values were later extrapolated to lithology-thickness scale using a number of reference points, which were marked

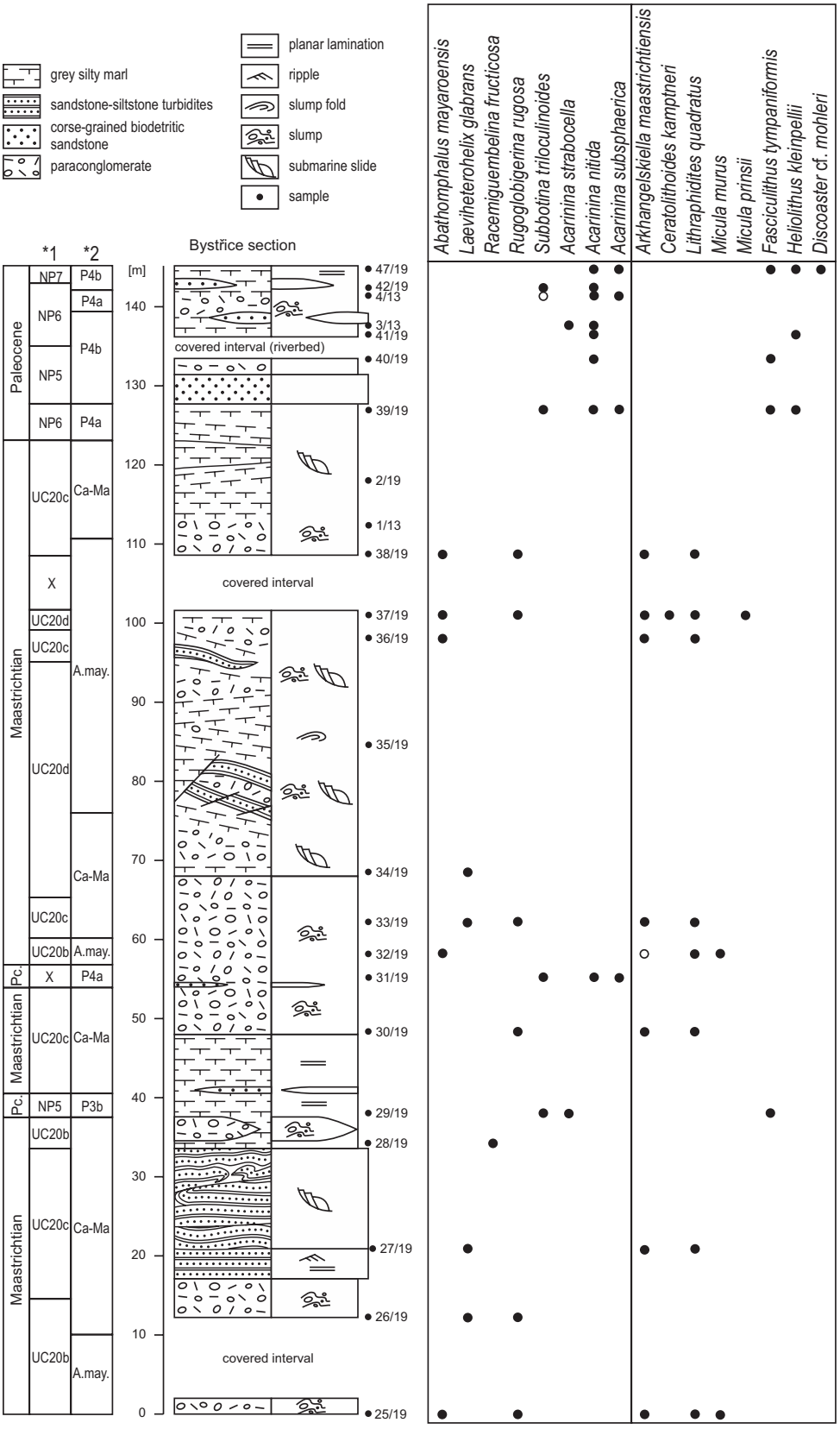

Fig. 2. Sedimentological log of the Bystřice section and biostratigraphically significant foraminifers and calcareous nannofossils. *1 – Calcareous nannofossil zones sensu Martini (1971) and Burnett (1998); *2 – planktonic foraminifer zones: A. may – *Abathomphalus mayaroensis*, Ca–Ma – unzoned Campanian–Maastrichtian; Paleocene zones sensu Olsson et al. (1999).

along the section. Additionally, a total of 86 samples were collected for laboratory analyses at the Laboratory of Paleomagnetism, Institute of Geology of the Czech Academy of Sciences. The laboratory measurements of MS, along with its anisotropy (AMS), field- (10–700 A/m) and frequency dependence (976 Hz to 15.6 kHz), were conducted with AGICO MFK1-FA kappabridge. The natural remanent magnetisation (NRM) and its alternating field demagnetisation (AF; up to 120 mT in 2–10 mT intervals) was measured using the 2G Superconducting Rock Magnetometer 755 (2G SRM). The AF-demagnetisation results were subjected to the principal component analysis (Kirschvink 1980) using the Remasoft program (Chadima & Hrouda 2006). Furthermore, several samples were also, after AF-demagnetisation, progressively magnetised up to 2.5 T and then stepwise demagnetized (≤120 mT) for isothermal remanent magnetisation (IRM). The S-ratios were acquired by saturating the samples in a high field (2.5 T) and then applying a back-field of 300 mT. Both IRM and S-ratios were obtained using an AGICO LDA-5/PAM1 and/or Magnetic Measurements pulse magnetiser (MMPM10) in conjunction with an AGICO JR-6 spinner magnetometer.

Total organic carbon (TOC), total inorganic carbon (TIC), and total Sulphur (TS) were measured using an ELTRA 2000 elemental analyser. FeO and Fe_2O_3 were measured by wet chemistry and flame atomic absorption spectroscopy (FAAS). Saturated and aromatic hydrocarbons were analysed using gas chromatography – mass spectrometry (GC–MS), while compound identification was based on mass spectra and suitable reference samples. Geochemical interpretation is based on peak area ratios. Isotopic composition of carbonate carbon and oxygen ($\delta^{13}C$ and $\delta^{18}O$) was measured on carbonate samples exposed to 100 % H_3PO_4 at 25 °C following McCrea (1950). The measurement of C and O isotopic compositions of the resultant CO_2 gas was performed using a DeltaV IRMS (Delta V Advantage Isotope Ratio Mass Spectrometer) in the Laboratories of the Czech Geological Survey in Prague. The accuracy of the measurement was checked by analyses of the international standard (IAEA) NBS 18 ($\delta^{13}C$=−5.014 ‰, $\delta^{18}O$=−23.2 ‰) and two in-house standards: Carrara marble ($\delta^{13}C$=2.29 ‰, $\delta^{18}O$=−1.32 ‰) and CS 2 ($\delta^{13}C$=2.93 ‰, $\delta^{18}O$=−3.86 ‰). Oxygen and carbon isotope ratios are reported in delta notation (δ) in per mil, relative to the V-PDB international standard. Overall analytical uncertainty was ±0.1 ‰ for both $\delta^{13}C$ and $\delta^{18}O$ values.

Results

Calcareous nannofossils

Poorly preserved and mostly fragmented nannofossils were found in a total of 17 samples (Electronic supplement S1). Overall nannofossil abundance varies in the Cretaceous strata between 1 and 15 specimens per field of view (FOV), whereas in the Paleocene, between 1 specimen per 20 FOV and 10 specimens per FOV.

Nannofossils in samples 25/19 to 28/19, 30/19 and 32/19 to 38/19 represent high-latitude Maastrichtian assemblages with dominance of *Micula staurophora* and the presence of cold-water preferring taxa *Prediscosphaera stoveri* and *Arkhangelskiella maastrichtiensis* (Fig. 3). Low-latitude Tethyan species *Micula murus*, *M. prinsii,* and *Ceratolithoides kamptneri* were detected occasionally only in a few samples (Fig. 2). The assemblages contain K–Pg survivor taxa (sensu Burnett 1998): *Markalius inversus, M. apertus, Cyclagelosphaera* div. spec., *Goniolithus fluckigeri, Zeugrhabdothus sigmoides, Neocrepidolithus cohenii,* and others.

Nannofossils in samples 29/19, 39/19 to 41/19 and 47/19 are Paleocene in age and include the stratigraphically-important species *Fasciculithus tympaniformis, F. involutus, Heliollithus kleinpelii, Sphenolithus anarrhopus, Toweius occultatus, Neochiastozygus junctus,* and *Discoaster mohleri* (Fig. 4). Specimens reworked from Upper Cretaceous strata are rare in those samples.

Foraminifers

All samples contained relatively rich and diversified foraminifer fauna with benthic taxa prevailing over planktonic. Calcareous benthic taxa prevail over agglutinated. The number of benthic foraminifers varies usually between 160 and 450 specimens in 1 g of rock. The proportion of planktonic taxa within foraminiferal taphocoenoses varies between 18 and 62 %, with the average value of 36 %.

In diversified planktonic-foraminifer assemblages, 33 Cretaceous and 25 Paleocene taxa were identified (Electronic supplement S2). The samples are dominated either by Cretaceous or Paleocene taxa, although each sample contains some reworked older species. The Cretaceous assemblages are characterised by dominant or abundant *Heterohelix globulosa* accompanied by frequent *Globigerinelloides asper* and *Guembelitria cretacea*. Globotruncanids are represented usually by rare *Globotruncana arca* and *Abathomphalus mayaroensis* (Fig. 5). The Paleocene assemblages are dominated usually by *Acarinina nitida*, accompanied by abundant *Subbotina patagonica, S. cancellata, S. velacoensis, Parasubbotina varianta, Morozovella praeangulata*, and *M. apanthesma* (Fig. 6).

All benthic foraminifer assemblages are dominated by calcareous taxa. Maastrichtian assemblages are characterised by the frequent occurrence of genera *Nonion, Praebulimina, Pyramidina, Siphonodosaria, Strictocostella, Quadrimorphina, Chilostomella, Cibicidoides, Gavelinella, Gyroidinoides, Alabamina, Lenticulina, Laevidentalina, Quinqueloculina, Fissurina*. Some samples contain as a minor component also bathyal agglutinated foraminifers of the genera *Gaudryina, Marssonella, Dorothia, Spiroplectammina,* as well as flysch-type forms of the genera *Rhizammina, Hyperammina, Ammodiscus, Thalmannammina* and *Remesella*. Common components of washed residues are calcitic prisms of inoceramids and echinoid spines.

The most frequent benthic genera in Paleocene assemblages are *Anomalinoides, Cibicidoides, Alabamina, Alabaminoides,*

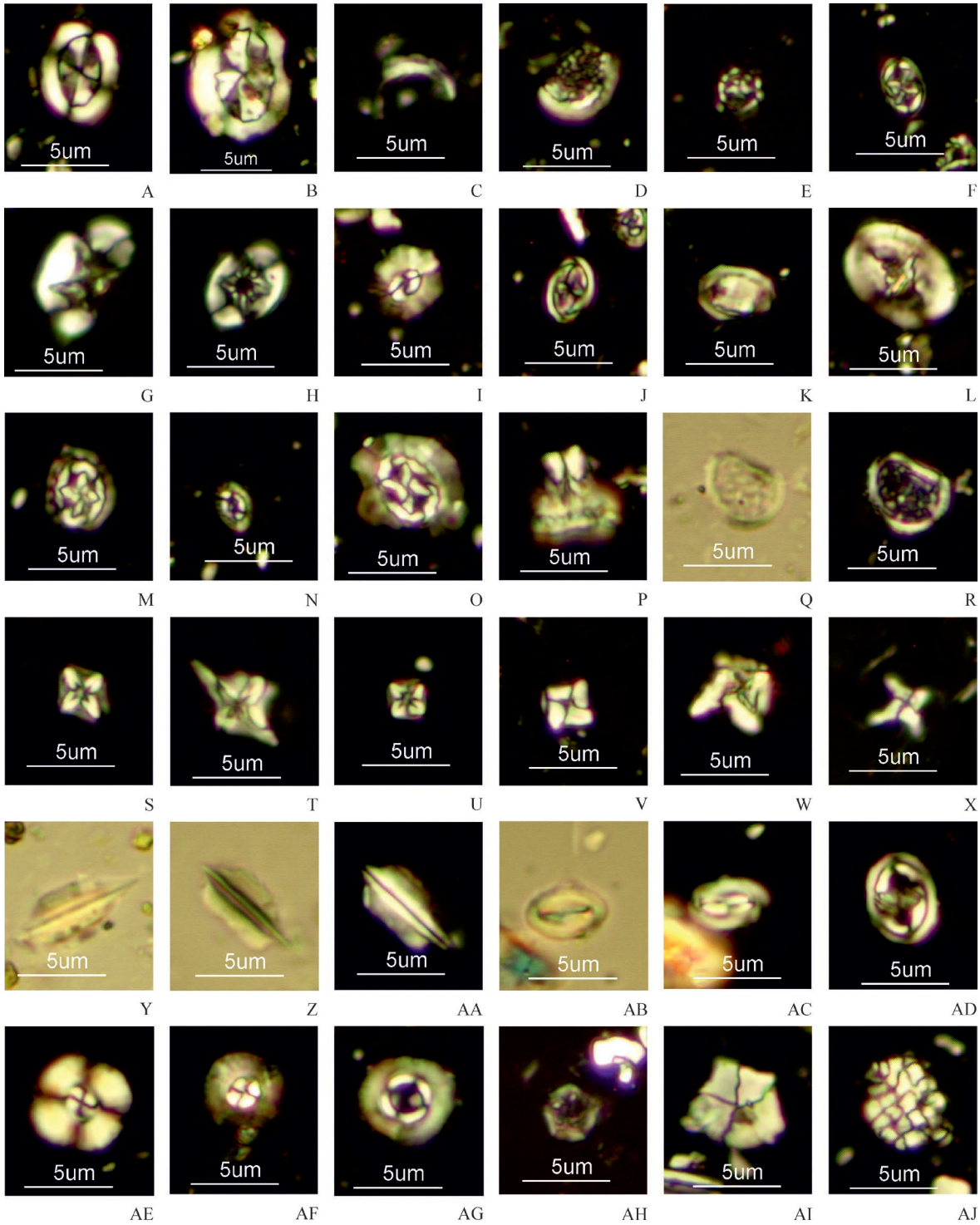

Fig. 3. Maastrichtian calcareous nannofossils including KT survivor taxa. **A** — *Arkhangelskiella confusa*, 28/19; **B** — *Arkhangelskiella maastrichtiensis,* 36/19; **C** — *Cribrosphaerella daniae* (outer rim, fragment), 37/19; **D** — *Cribrosphaerella ehrenbergii* (fragment of the large broadly elliptical specimen), 35/19; **E** — *Corollithion exiguum*, 37/19; **F** — *Corollithion madagaskarensis*, 33/19; **G** — *Eiffellithus pospichalii*, 37/19; **H** — *Eiffellithus parallelus*, 35/19; **I** — *Biscutum melaniae*, 37/19; **J** — *Staurolithites laffittei*, 35/19; **K** — *Reinhardtites* cf. *elkefensis*, 34/19; **L** — *Reinhardtites levis* (reworked specimen from the older Campanian strata), 35/19; **M** — *Prediscosphaera* cf. *arkhangelskyi,* 33/19; **N** — *Prediscosphaera stoveri*, 28/19; **O** — *Prediscosphaera microrhabdulina*, 28/19; **P** — *Prediscosphaera majungae*, 36/19; **Q**, **R** — *Nephrolithus frequens*, 27/19; **S** — *Micula staurophora*, 27/19; **T** — *Micula concava,* 32/19; **U** — *Micula cubiformis*, 37/19; **V** — *Micula murus*, 25/19; **W** — *Micula murus-prinsii*, 32/19; **X** — *Micula prinsii,* 37/19; **Y**–**AA** — *Lithraphidites quadratus*, 25 – 38/19, 26, 27 – 33/19. KT survivor species: **AB**, **AC** — *Neocrepidolithus cohenii,* 33/19; **AD** — *Zeugrhabdotus sigmoides*, 33/19; **AE** — *Cyclacelosphaera margerelii*, 33/19; **AF** — *Markalius inversus*, 26/19; **AG** — *Markalius apertus*, 27/19; **AH** — *Gonilolithus fluckigeri*, 35/19; **AI** — *Braarudosphaera bigelowii bigelowii*, 34/19; **AJ** — *Thoracosphaera* sp., 35/19. Q, Y, Z, AB – plane-polarized light; the rest in cross-polarized light.

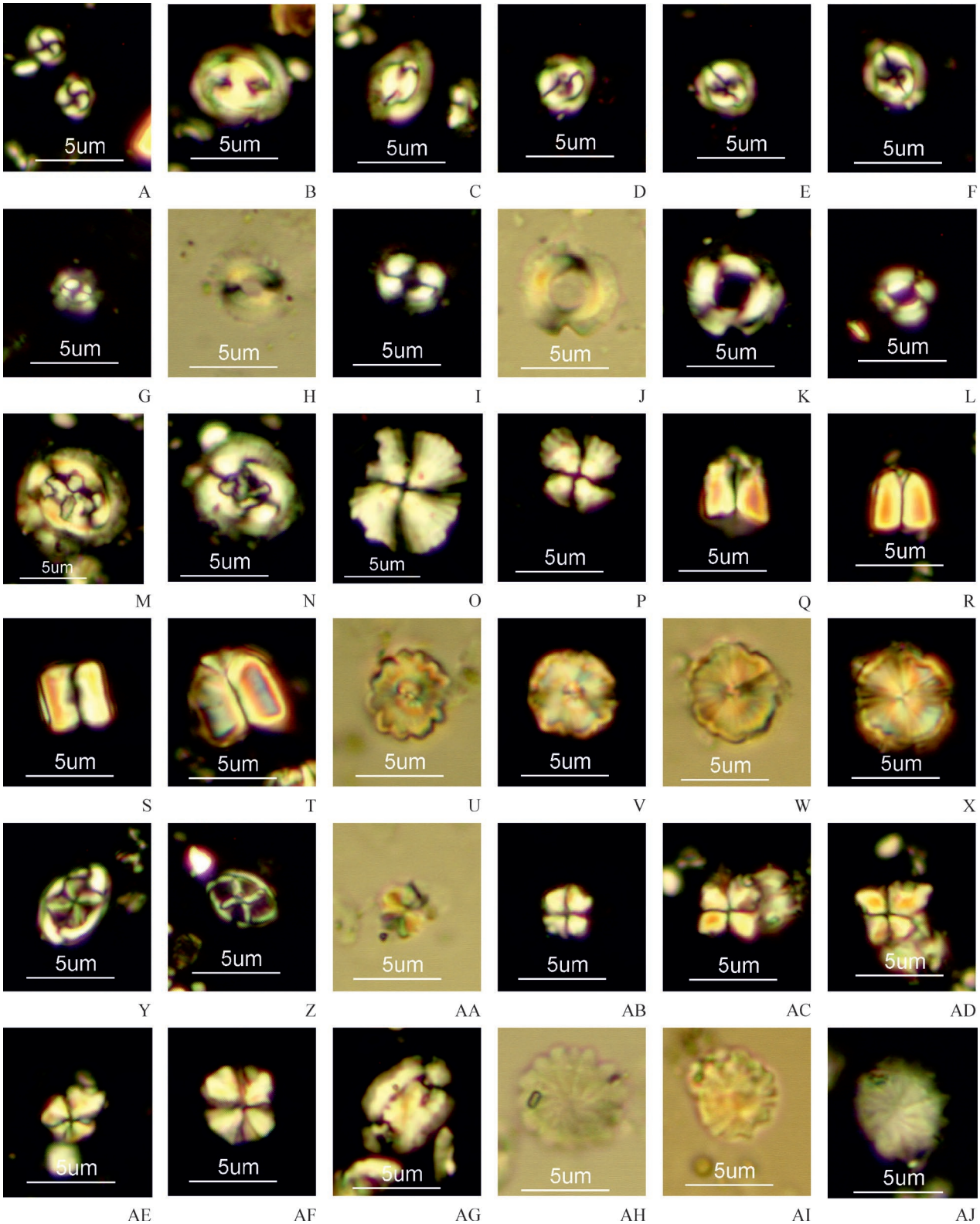

Fig. 4. Thanetian and Selandian calcareous nannofossils. **A** — *Toweius rotundus,* 47/19; **B**, **C** — *Toweius occultatus,* 47/19; **D**, **E** — *Toweius pertusus,* 47/19; **F** — *Toweius tovae*, 47/19; **G**–**I** — *Coccolithus pelagicus,* G: 27/19, H, I: 39/19; **J**, **K** — *Ericsonia subpertusa*, 40/19; **L** — *Reticulofenestra* sp., 47/19; **M** — *Cruciplacolithus tenuis*, 47/19; **N** — *Chiasmolithus bidens,* 47/19; **O**, **P** — *Heliolithus kleinpellii*, O: 39/19, P: 41/19; **Q**, **R** — *Fasciculithus tympaniformis*, Q: 29/19, 18: 39/19; **S**, **T** — *Fasciculithus involutus*, 47/19; **U**–**X** — *Fasciculithus* sp. (cross section), U, V: 40/19, W, X: 47/19; **Y** — *Neochistozygus saepes*, 47/19; **Z** — *Neochiastozygus modestus*, 47/19; **AA**, **AB** — *Sphenolithus primus*, 40/19; **AC**–**AE** — *Sphenolithus anarrhopus*, 47/19; **AF** — *Sphenolithus moriformis,* 41/19; **AG** — *Ellipsolitus distichus*, 47/19; **AH**–**AJ** — *Discoaster mohleri*, 47/19. H, J, U, W, AA, AH, AI – plane- polarized light; the rest in cross-polarized light.

Gyroidinoides, Laevidentalina, Nonion, Gavelinella, Lenticulina, Tappanina, Aragonia, Globulina, Nuttallinella, and *Karreria*. Subordinate agglutinated taxa are represented by bathyal taxa (*Dorothia, Marssonella, Spiroplectinella, Arenobulimina, Hagenowella*), but also flysch-type forms (*Rhizammina, Bathysiphon, Hyperammina, Nothia, Glomospira, Arthrodendron, Caudammina, Rzehakina, Haplophragmoides, Recurvoides, Karrerulina, Spiroplectammina*). Pyrite casts of diatoms are a common characteristic component of Paleocene washing residues.

Sedimentology

Paraconglomerates (pebbly mudstones) represent the dominant lithology in the Bystřice section. Clasts, 1 cm to 2 m in diameter, vary in shape from well-rounded to angular and are composed of exotic metamorphic rocks, Devonian and Mississippian limestones, sandstones, black coal, coal shale, and carbonate concretions. Small quartz and chert pebbles usually have a polished surface. They are arranged chaotically in the prevailing matrix and their share ranges approximately between 5 and 50 %. The matrix is grey silty and sandy calcareous claystone, as well as marl. Thick bodies of paraconglomerates can be classified as slumps. Frequent slump folds in the matrix as well as in marly intraclasts indicate synsedimentary deformation (Fig. 7B).

Up-to 20 m thick paraconglomerate bodies are separated by bedded grey silty claystones and marls (Fig. 7D). Locally shale-pebble conglomerates can be seen. In places, sequences of medium-rhythmic sandstone flysch occur as well. The 16 m thick sandstone sequence in the lower part of the section (Fig. 7C) consists of classical turbidites with $T_{a–d}$ intervals. Some sandstone beds contain abundant bioturbation (*Thalassinoides, Scolicia, Chondrites, Palaeodictyon, Arthrophycus, Rhizocorallium, Ophiomorpha*).

Folded and thrusted sandstone beds, breccia of partly-lithified sandstones, and characteristic failure planes (Fig. 7D) indicate sliding (submarine landslides).

In the lower part of the section, stratigraphical repetition was encountered based on biostratigraphy. Sediments with Maastrichtian foraminifers and nannofossils prevail, although in two levels, Paleocene microfossils were found. Both Maastrichtian and Paleocene assemblages are strictly separated, except for a small number of Cretaceous microfossils in Paleocene samples.

The upper part of the section (Selandian) comprises grey silty and sandy claystones with local 1 to 4 m thick lenticular bodies of coarse-grained calcareous sandstones and pebbly to cobbly calcareous petromictic conglomerates. A characteristic feature of sandstones and conglomerates is algal detritus. Several-metre thick paraconglomerates contain up to 2 m large boulders of exotic rocks, including Paleocene limestones with mollusc macrofauna.

The prevailing grey marly lithology of the entire section allows assignment to the Frýdek Formation. Grey calcareous claystones at the top of the section contain 10 to 20 cm thick layers of greenish-grey bioturbated marlstone with *Chondrites*. They mark the base of the overlying Frýdlant Formation.

Geochemistry

The predominant lithofacies in the Bystřice section are shales and marl with a varying proportion of calcite. The $CaCO_3$ content ranges from 4.83 to 69.91 wt. % in the upper Paleocene interval and from 9.33 to 31.17 wt. % in the Maastrichtian. Total organic carbon (TOC) values range from 0.50 to 1.53 wt. % in the Paleocene and from 0.81–1.56 wt. % in the Maastrichtian. The FeO/Fe_2O_3 ratio shows the highest values at sample positions of 17.1, 55.2, 68.5, and 144.84 m.

Chromatography of extractable organic matter (EOM) provides proxy parameters of the probable biological origin of EOM, such as carbon preference index (CPI) values, which vary from 2.02 to 2.54. Relative proportion of organic matter originating from terrestrial plants and aquatic lower plants is evaluated using the TAR index.

Stable isotopes of carbon and oxygen in bulk carbonate ($\delta^{13}C$ and $\delta^{18}O$) show a significant shift of both $\delta^{13}C$ and $\delta^{18}O$ parameters to more negative values, which occurs at a depth of 38.09, 55.21, and partially at 126.93 and 133.43 m. For analytical data and numerical proxy parameters, see the Electronic supplement S3.

Magnetic properties

The magnetic susceptibilities (MS) of samples indicate paramagnetic values with average value 93 μSI in the entire Bystřice section (Fig. 8B). The observed small-scale variations correspond seemingly to lithology changes.

MS values measured *in situ* along the section during the fieldwork correspond well with laboratory measured susceptibilities and display similar trends. Specimens indicate relatively low frequency dependence (around 2 %) of magnetic susceptibility in the lower part of the section. However, FD up to 7 % and thus more superparamagnetic particles can be observed in the second half of the section and show a decreasing trend towards Paleocene (Fig. 8E). Samples display either very minor field dependency of magnetic susceptibility or none at all, which probably reflects magnetite as the main magnetic fraction.

This observation is supported by the S-ratios over 0.9, as well as acquisition of isothermal remanence, indicating that over 50 % of magnetisation is gained already by 50 mT and magnetic saturation (SIRM) is obtained between 0.15–0.5 T, which is typical behaviour for samples containing magnetite. Only 1 sample showed lower S-ratio and no SIRM by 2.5 T, indicating the presence of high coercivity fraction, such as hematite or goethite (Fig. 8G–H). Moreover, the positive correlation between IRM and MS (Fig. 8I) indicates that variations in susceptibilities depend on the concentration rather than (magneto)mineralogical changes. Samples display a mostly oblate shape of magnetic fraction (Fig. 8D, J) and relatively low degree of AMS (average 4 %; Fig. 8C)

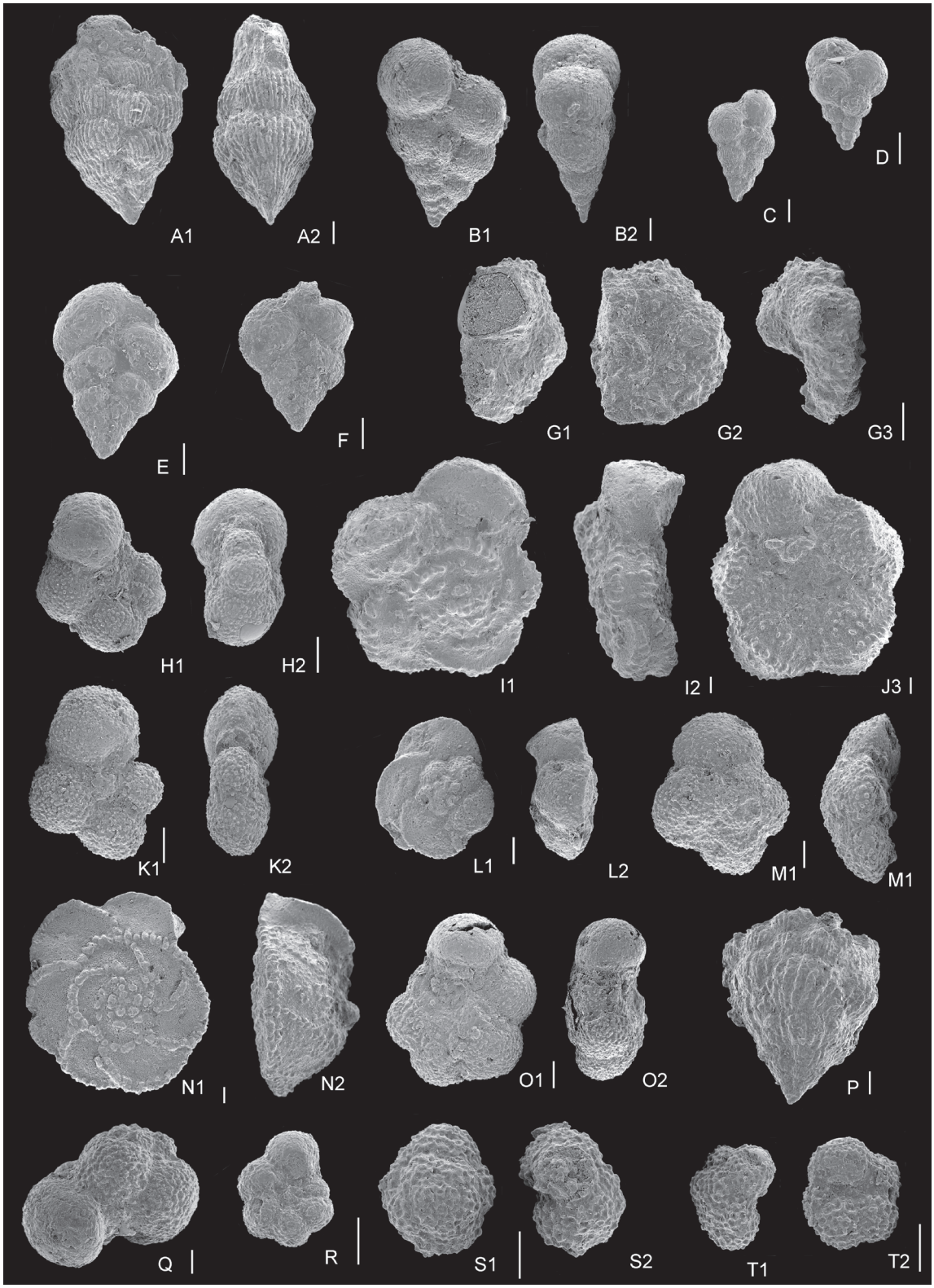

Fig. 5. Cretaceous and Danian foraminifers. **A1**, **A2** — *Planoglobulina brazoensis*, sample 38/19; **B1**, **B2** — *Heterohelix labellosa*, 33/19; **C** — *Heterohelix globulosa*, 1/13; **D** — *Guembelitria cretacea*, 1/13; **E** — *Laeviheterohelix dentata*, 1/13; **F** — *Laeviheterohelix glabrans*, 33/19; **G1**–**G3** — *Dicarinella canaliculata*, 3/13; **H1**, **H2** — *Globigerinelloides asper*, 1/13; **I1**– **I3** — *Abathomphalus mayaroensis*, 35/19; **K1**, **K2** — *Globigerinelloides subcarinatus*, 33/19; **L1**, **L2** — *Globotruncana aegyptiaca*, 35/19; **M1**, **M2** — *Globotruncanella petaloidea*, 34/19; **N1**, **N2** — *Globotruncanita angulata*, 35/19; **O1**, **O2** — *Rugoglobigerina hexacamerata*, 33/19; **P** — *Racemiguembelina fructicosa*, 28/19; **Q** — *Rugoglobigerina milamensis*, 25/19; **R** — *Hedbergella planispira*, 1/13; **S1**, **S2**, **T1**, **T2** — *Eoglobigerina edita*, 39/19. Scale bars=0.5 um.

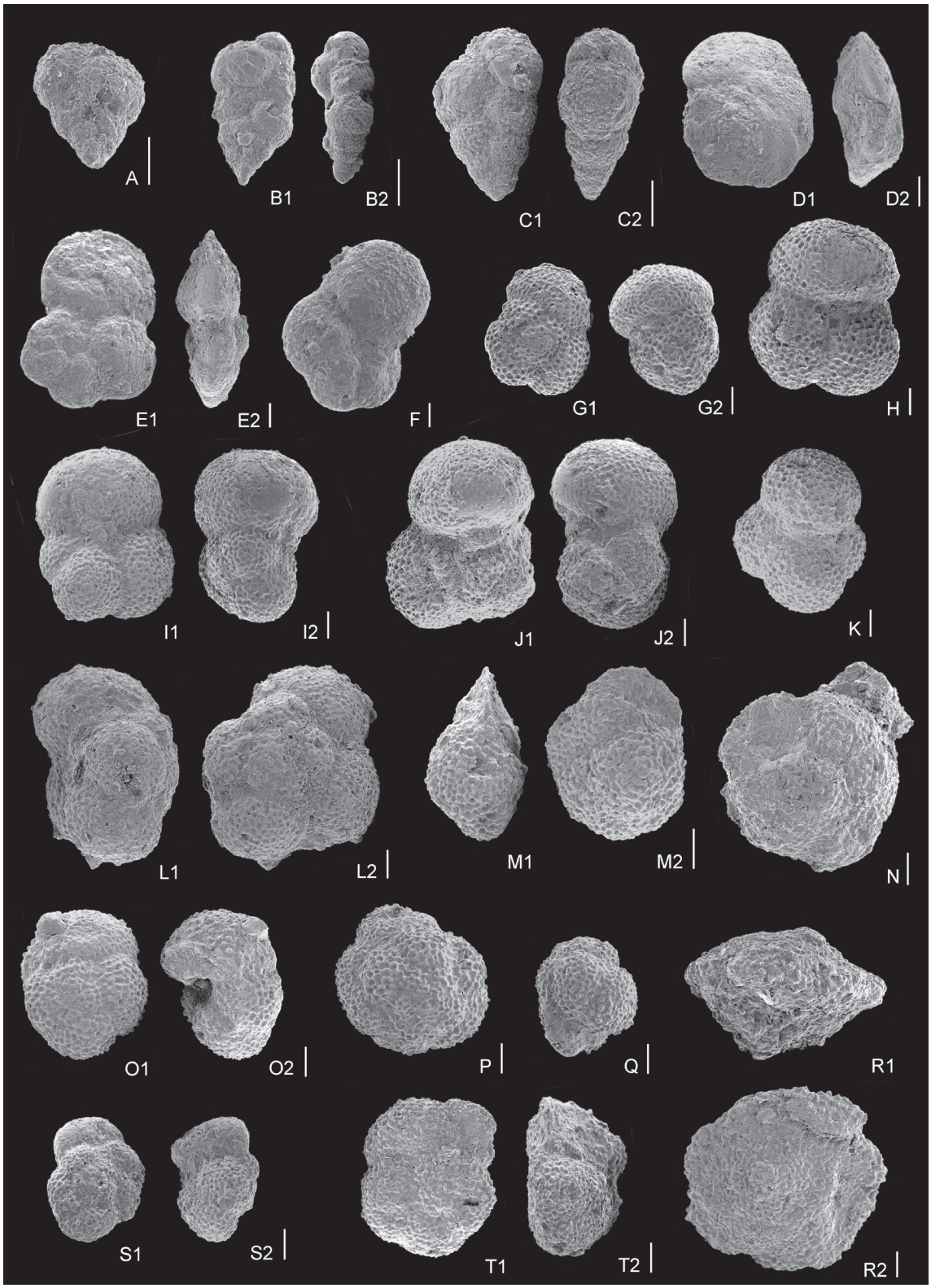

Fig. 6. Selandian foraminifers. **A** — *Chiloguembelina crinita*, sample 47/19; **B1**, **B2** — *Chiloguembelina morsei*, 47/19; **C1**, **C2** — *Chiloguembelina trinitatensis*, 47/19; **D1**, **D2** — *Globanomalina pseudomenardii*, 47/19; **E1**, **E2**, **F** — *Globanomalina chapmani*, 47/19; **G1**, **G2**, **H** — *Subbotina velascoensis*, 39/19; **I1**, **I2** — *Subbotina patagonica*, 31/19; **J1**, **J2** — *Subbotina triloculinoides*, 39/19; **K** — *Subbotina cancellata*, 39/19; **L1**, **L2** — *Parasubbotina varianta*, 40/19; **M1**, **M2** — *Igorina albeari*, 39/19; **N** — *Acarinina strabocella*, 29/19; **O1**, **O2** — *Acarinina nitida*, 39/19; **P**, **Q** — *Acarinina subsphaerica*, 39/19; **R1**, **R2** — *Morozovella acutispira*, 31/19; **S1**, **S2** — *Morozovella praeangulata*, 29/19; **T1**, **T2** — *Morozovella apanthesma*, 3/13. Scale bars=0.5 um.

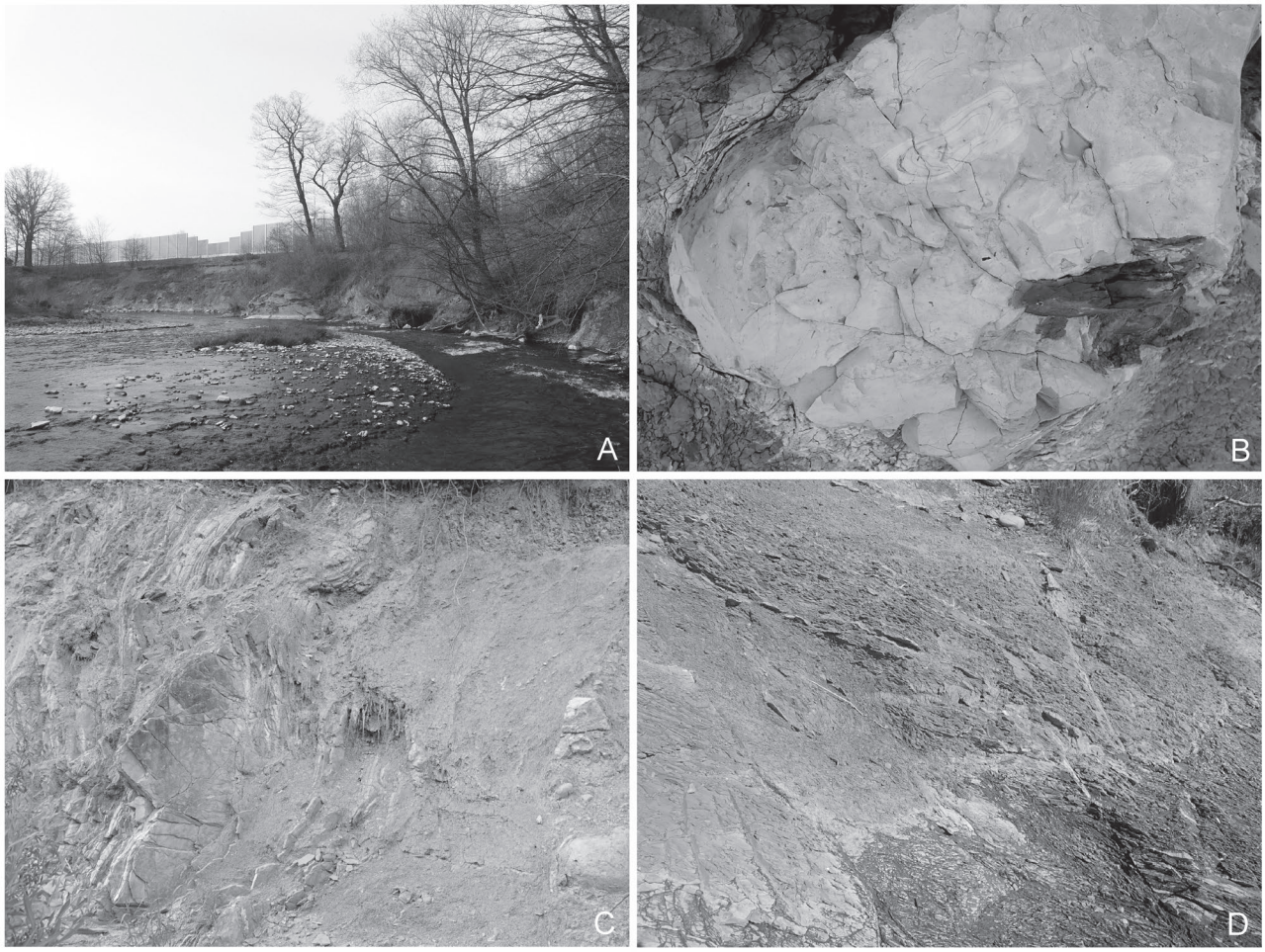

Fig. 7. Bystřice section, Frýdek Formation, Subsilesian Unit. **A** — overall view; **B** — slump folds in large intraclast of marlstone (diameter of block ca 1 m); **C** — sequence of sandstone turbidites on the left and marls with paraconglomerate (slump) on the right (width of view ca 5 m), **D** — grey marls with numerous sliding planes (width of view ca 1 m).

throughout the section, with only occasional higher values, and does not show any correlation to MS variations.

Like MS, the natural remanent magnetisation (NRM) of specimens predominantly indicate low values (NRM=0.86 mA/m). The alternating field (AF) demagnetisation of the samples showed that remanence is mostly removed by 60 mT (median destructive field 10–15 mT), which indicates that the low coercivity fraction, such as magnetite, is the carrier of the remanence. Occasionally, the samples were slightly more resistant to the alternating field.

The multicomponent analysis of paleomagnetic data revealed the presence of one or two magnetic components. The first component (component A; viscous; declination D=359°, inclination I=71°; geographic coordinates) is present in most of the samples and is very close to the present Earth field. The second component holds dual polarity (normal C_N: D=99°, I=66° and reversed C_R: D=93°, I=−71°) and occurs within a wide AF-range from 6–35 mT to 15–65 mT (occasionally up to 120 mT). Unfortunately, the C_N occurs occasionally quite close to the A-component and quite likely displays strong influence of remagnetisation. Furthermore, both C_N and C_R display wide scatter (k=2.6 and 2.3; A95=20° and 23°, dp=26° and 34°, dm=32° and 39°, respectively) and are not antipodal. Due to strong remagnetisation and the absence of clear primary magnetisation component, the data are not used to generate the magnetostratigraphy.

Discussion

Biostratigraphy

In general, the stratigraphy established using calcareous nannofossils corresponds well with that based on planktonic foraminifers (Figs. 2 and 9). The Cretaceous nannofossil assemblages were assigned to the upper Maastrichtian zone UC20, which is defined by the presence of *Lithraphidites quadratus.* The same samples contain the upper Maastrichtian index foraminifer species *Abathomphalus mayaroensis*.

While the youngest Maastrichtian foraminifer zones *Pseudoguembelina hariaensis* and *Plummerita hantkeninoides* cannot be identified due the lack of index species,

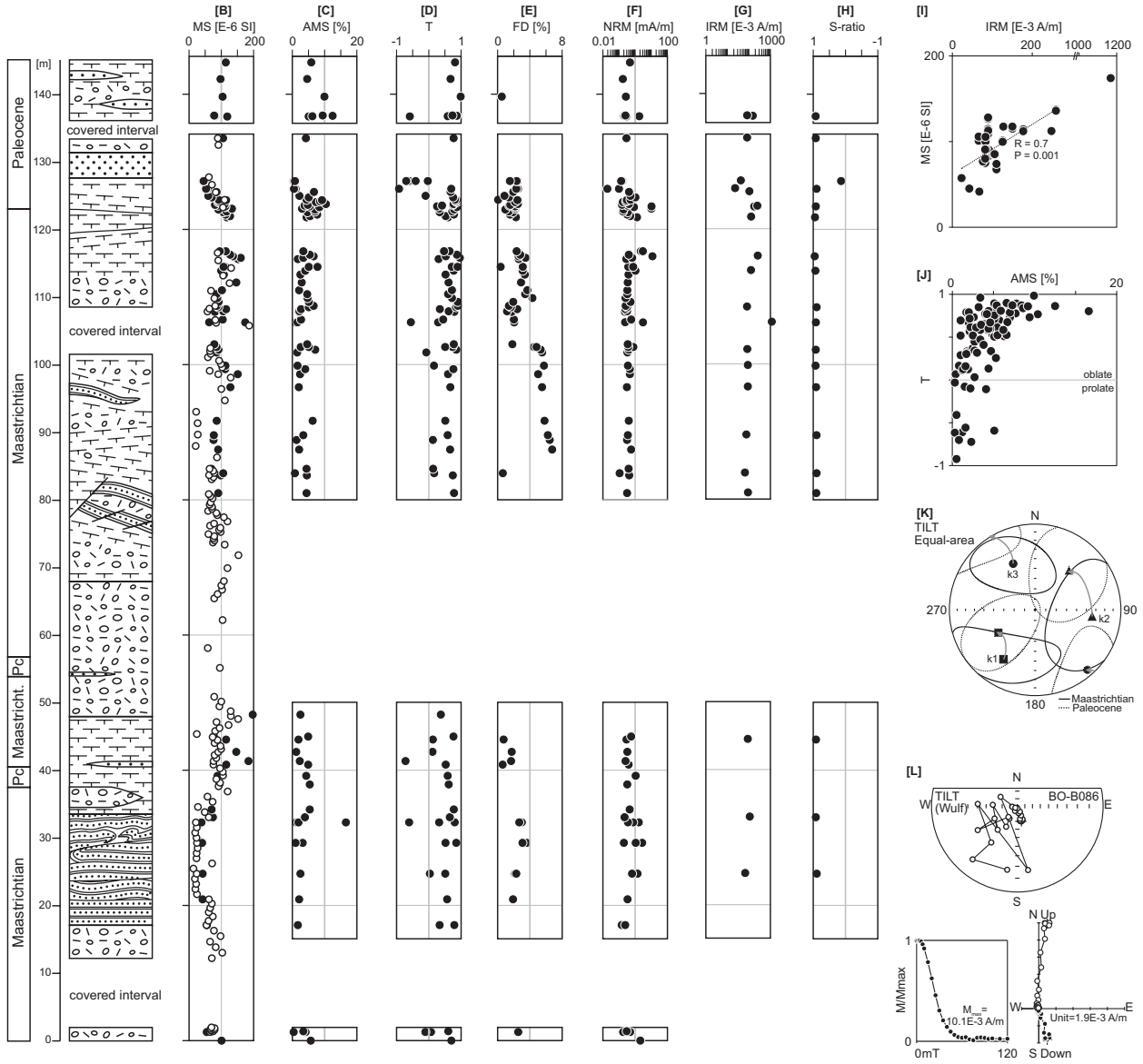

Fig. 8. Magnetic properties along Bystřice nad Olší section. **A** — Lithology (Maastricht. – Maastrichtian; Pc. – Paleocene); **B** — magnetic susceptibilities (MS) measured in laboratory (filled symbols) and in-situ in the field (empty symbols); **C** — degree of anisotropy of magnetic susceptibility (AMS); **D** — shape factor (T); **E** — frequency dependence of magnetic susceptibility (FD); **F** — natural remanent magnetisation (NRM); **G** — isothermal remanent magnetisation at 2.5 T (IRM); **H** — S-ratio; **I** — correlation between MS and IRM; **J** — AMS vs T plot; **K** — tilt-corrected equal area projection of the AMS. Symbols indicate the mean values of maximum (k1), intermediate (k2), and minimum (k3) susceptibility axes and their 95 % error ellipses. Grey arrows illustrate change in AMS axes between Maastrichtian (solid lines) and Paleocene (dashed lines) samples. **L** — Example of alternating field demagnetisation: stereographic projection (up), orthogonal (Zijderveld) vector projection (down, right), and magnetisation intensity curves (down, left).

the nannofossils allow subdivision of the UC20 zone into subzones. *Micula murus* indicates the zone UC20b^{TP}, *Arkhangelskiella maastrichtiensis* the zone UC20c^{BP}, and *Ceratolithoides kamptneri* the zone UC20c^{TP}. The uppermost Maastrichtian *Micula prinsii* zone UC20d^{TP} was encountered in a single sample (37/19). The influx of the *Corollithion exiguum* defined as the secondary event within the boreal UC20d^{BP} zone in Europe by Burnett (1998) was not recorded.

The Selandian is documented by the occurrence of nannofossil *Fasciculithus tympaniformis*, NP5 zone in the samples 29/19 and 40/19, and by *Heliolithus kleinpellii*, zone NP6 in 39/19 and 41/19. The Selandian–Thanetian boundary is placed within the NP6 zone (Varol 1998; Luterbacher et al. 2004). The sample 47/9 is assigned to the Thanetian zone NP7 based on the presence of *Discoaster mohleri*.

Paleocene foraminifer biostratigraphy in the section is complicated by the fact that all of the samples contain a certain amount of older redeposited taxa. The P3b zone was identified in the sample 29/19 based on the frequent occurrence of *Acarinina strabocella* and *Subbotina triloculinoides*. The zone

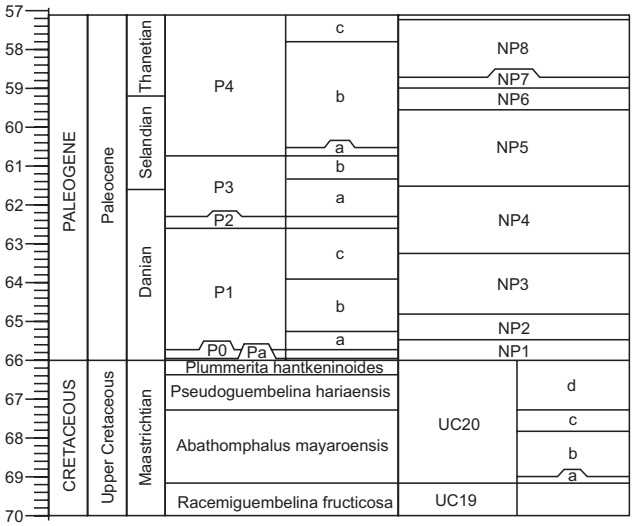

Fig. 9. Correlation of standard foraminifer and nannofossil biozones.

P4a was recognised in the samples 31/19, 39/19, and 4/13 based on the abundant occurrence of *Acarinina nitida* and *A. subsphaerica*. The zone P4b, which was encountered in the upper part of the section, differs by the disappearance of *A. subsphaerica*.

Redeposition is common through the section and can be demonstrated on the sample 40/19. This sample contains a few Cretaceous taxa (*Heterohelix globulosa, Globigerinelloides asper*), rare *Eoglobigerina eobulloides* (P0–P1b; Danian), abundant *Morozovella praeangulata* (P2–P3a; Danian–Selandian), rare *Igorina pusilla* (P3; Selandian), and finally abundant *Acarinina nitida* (P4a–c), which together with a lack of *A. subsphaerica* allows assignment to the P4b zone (Selandian–Thanetian).

The redeposited foraminifers prove the existence of Danian sediments in the Subsilesian sector of the Silesian Basin. In the Bystřice section, the upper Maastrichtian and Selandian sediments are in immediate contact, however, Danian strata were in fact present higher in the paleoslope of the basin. On the other hand, a single find of *Dicarinella canaliculata* (Turonian–Santonian) in the Paleocene sample 3/13 documents the older Cretaceous history of the basin.

In general, stratigraphic interpretation of both calcareous nannofossils and planktonic foraminifers cannot rely on the sequence of bioevents, since mass flows formed a large part of the section. The youngest fossil in the sample does not necessarily help to establish the correct stratigraphic position of the sediments, since some parts of the section seem to be transported *en block* as submarine landslides.

Depositional environment

Paleocene sediments of the studied section generally show a lower calcite content and higher siliciclastic input than Maastrichtian sediments. This may indicate higher input of land-derived material. A partial inverse relationship between the carbonate content and total organic carbon (TOC) shows closer association of organic matter with clay mineral fraction of the rocks. The FeO/Fe_2O_3 ratio (Fig. 10, Electronic supplement S3) shows neither convincing correlation with TOC, nor with total sulphur (TS). The highest values of FeO/Fe_2O_3 occur at sample positions of 17.1, 55.2, 68.5, and 144.84 m regardless of stratigraphy. This proxy parameter indicates a relative change towards dysoxic conditions during deposition, as well as early diagenesis in the mentioned intervals of the profile.

Chromatography of extractable organic matter, mainly the carbon preference index (CPI) index ranging from 2.02 to 2.54, suggests that kerogen in the entire Bystřice section is thermally immature; the rocks did not experience a deeper burial and diagenetic temperatures did not exceed 80 °C. Low thermal maturity is a precondition for using the n-alkane distribution as a proxy parameter of origin of organic matter, e.g., based on terrestrial /aquatic ratio (TAR). Paleocene sediments show prevailing aquatic organic matter, while Maastrichtian shales together with the Paleocene sample at 127 m have a stronger terrestrial plant proxy signal (Fig. 11). The above-mentioned sample at 127 m also shows extremely high benthic foraminifer density, which may indicate an eutrophic event supported by terrestrial input (Fig. 11). While variations in magnetic susceptibilities seem to be lithologically dependent and indicate mostly the concentration of magnetite in the samples, average MS of the Maastrichtian samples (97 μSI) is slightly higher when compared to Paleocene (83 μSI) and could reflect slightly higher magnetite input during the Maastrichtian. Pristane/phytane ratio (Pri/Phy) is often used as a measure of oxic or dysoxic conditions in the depositional environment (Peters et al. 2004). A shift to more oxic conditions is observed in the Paleocene samples when compared with the Maastrichtian ones. In general, none of the samples are close to or less than 1, i.e., no true anoxic or strongly dysoxic conditions are observed in the profile. The differences in conclusions driven from Pri/Phy and FeO/Fe_2O_3 ratios are due to the fact that Pri/Phy is considered to be a measure of oxygen deficiency in the water column above the sea floor and does not change as much during slumping (Killops & Killops 2004), while FeO/Fe_2O_3 changes significantly within the first ten metres below the sediment surface and usually decreases during redeposition, if the water is sufficiently rich in oxygen.

Both carbon and oxygen isotopic composition of bulk carbonate show excursions to more negative values in the Paleocene samples: $\delta^{13}C < 0.5$ ‰ and $\delta^{18}O < -5.4$ ‰. The bulk carbonate values are affected by diagenetic recrystallization. Since the diagenetic history of both the Paleocene and Maastrichtian sediments was similar, the differences between Maastrichtian and Paleocene values should reflect the primary ratio. Paleoclimatic control of the isotopic composition of carbonates is generally interpreted by way of warming and increased humidity resulting in more negative $\delta^{18}O$ in the carbonate fossil shells, while cooling and aridification result in more positive values (e.g., Zachos et al. 2001, 2008; Edgar

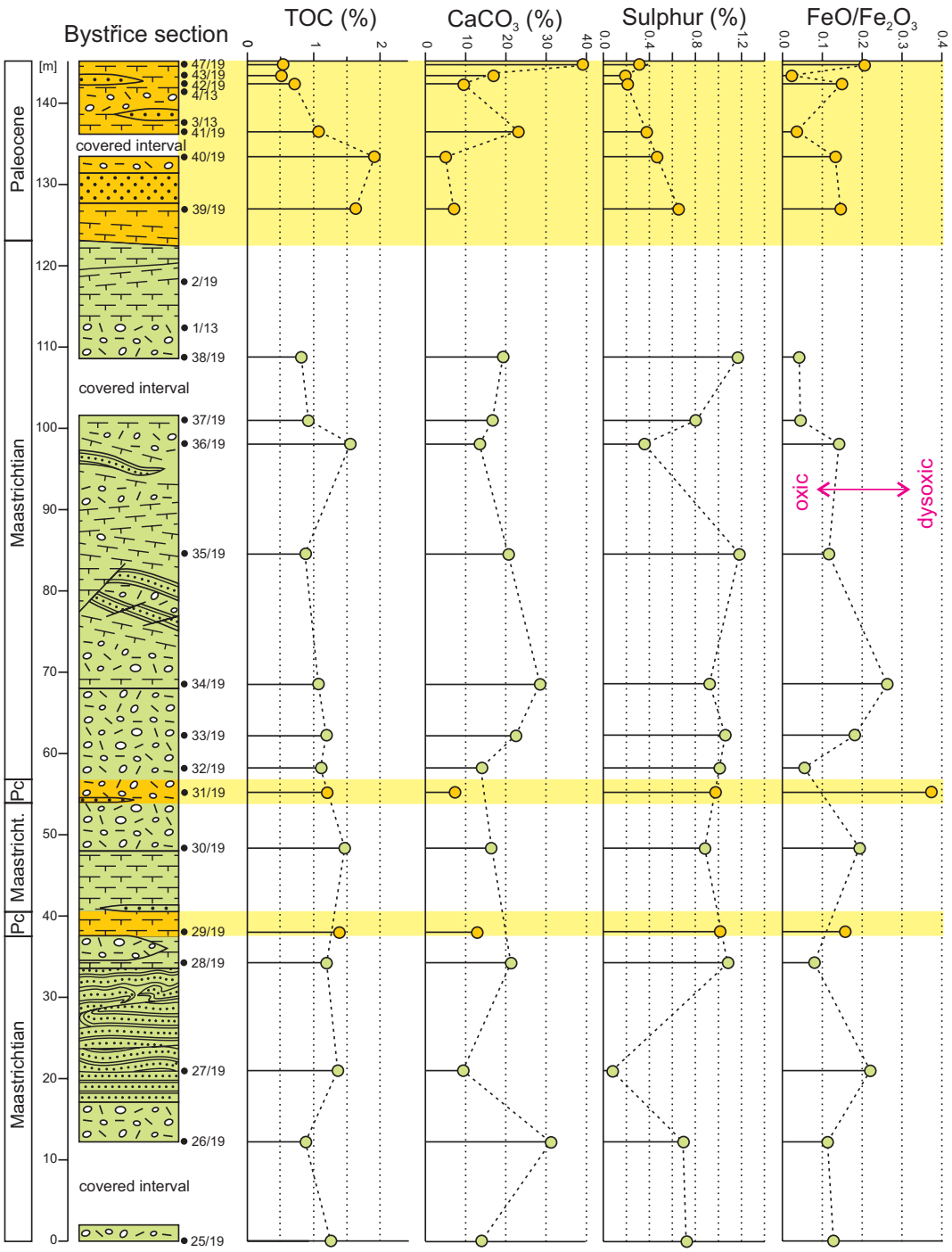

Fig. 10. Geochemical proxies across the Bystřice section.

et al. 2010). This would suggest that the climatic temperature was lower in the Maastrichtian and higher in the Selandian within the Subsilesian sector of the Silesian Basin. In the Paleocene samples, an inverse correlation is the observed between $\delta^{18}O$ and $\delta^{13}C$ values. These negative isotopic excursions correlate with lower values of terrestrial/aquatic ratio based on n-alkane TAR ratio in the profile (Fig. 11), i.e., with elevated aquatic organic matter.

Low-latitude species *Micula murus*, *M. prinsii*, and *Ceratolithoides kamptneri* (asterisks in Fig. 11) in otherwise cold-water Maastrichtian nannofossil assemblage may indicate warming of the surface waters caused by Deccan volcanism (Thibault & Gardin 2010; Thibault & Husson 2016; Wierzbicki & Kędzierski 2020; Švábenická 2022).

Abundant slumps, slides, and bathyal foraminifer biofacies indicate deposition on the basin slope in the bathyal zone.

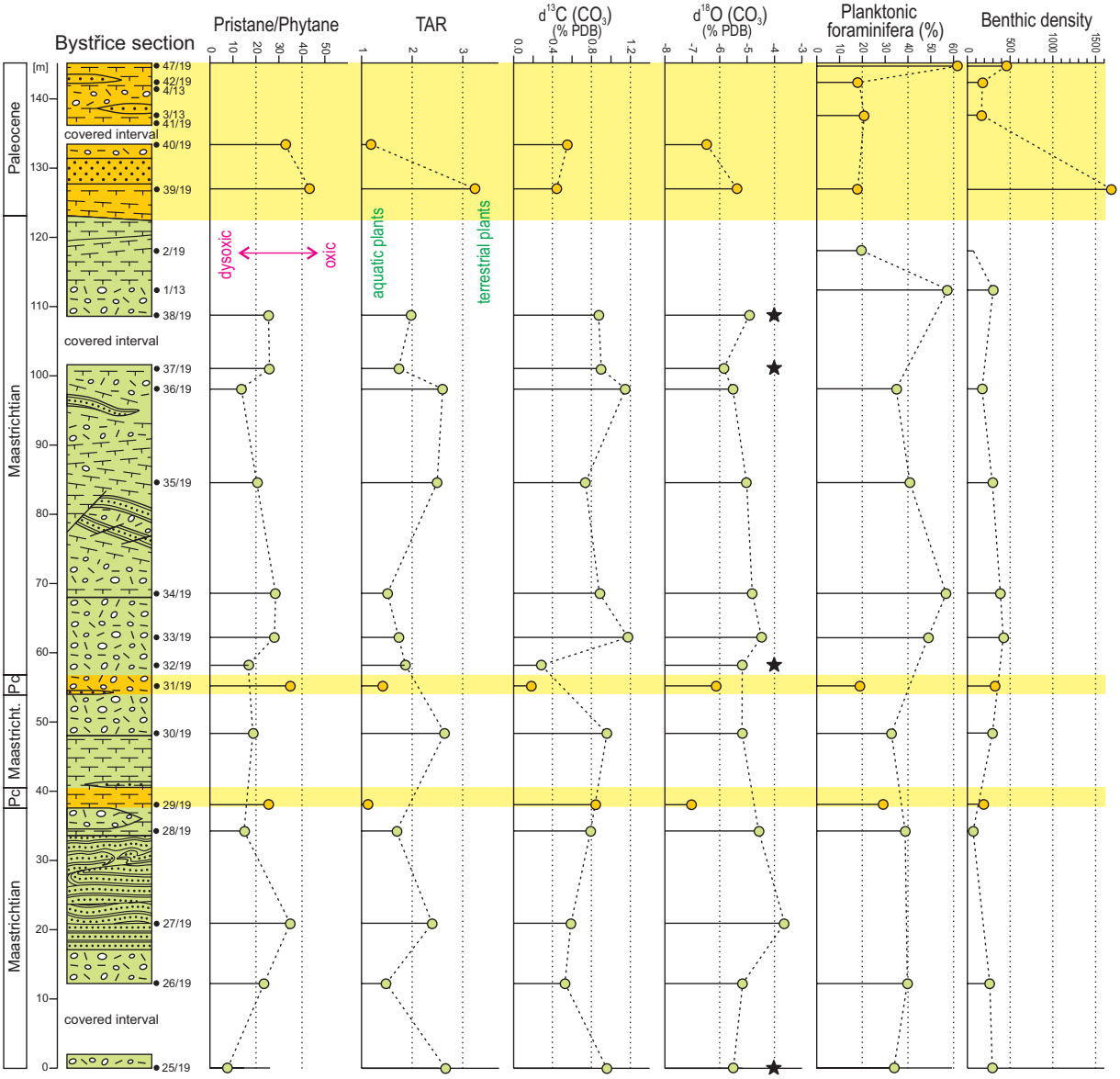

Fig. 11. Paleoenvironmental proxy parameters across the Bystřice section: pristane/phytane ratio of isoprenoid alkanes; TAR – terrestrial/aquatic ratio based on n-alkane distribution, $\delta^{13}C$ and $\delta^{18}O$ – carbon and oxygen isotopic composition of bulk carbonate. The occurrences of warm-water nannoplankton are indicated by asterisk. Benthic density calculated as number of benthic foraminifers per 1 gram of rock.

The polished quartz pebbles give evidence of thick and dense gravity flows which had exerted sufficient pressure for polishing the pebbles in the matrix and serving as a polishing agent. The paraconglomerates with Maastrichtian foraminifers and nannoplankton does not contain any Paleocene microfossils. This can be explained by transport in compact mass flow moving *en bloc* (probably submarine slide), without mixing with allochthonous Paleocene sediment. Therefore, it is quite likely that the paraconglomerates with exotic boulders were deposited in the late Maastrichtian, when they gained their chaotic structure and were subsequently redeposited during the Selandian. Slides and gravity folds may be considered a result of high sedimentary rate that caused paleoslope instability. Local sandstone bodies in the studied section possibly represent channel fills (channelised turbidites).

Stratigraphic repetition of Maastrichtian and Paleocene strata may be theoretically caused by both tectonic repetition or redeposition of Maastrichtian sediments during the Paleocene. The second explanation seems to be more probable in the studied section. Paleocene strata generally show a normal stratigraphic sequence of biostratigraphic zones. In the sediments with Maastrichtian microfauna, the nannofossil biozones changes from sample to sample rather chaotically (Fig. 2). It is not clear whether the strata with the Maastrichtian microfossils at the base of the section are true Maastrichtian

or rather slump and slide bodies composed of Maastrichtian sediments reworked during the Paleocene.

While sedimentary features and microfauna mainly indicate redeposition by slumping and sliding, the magnetic fabrics suggests a probable influence of tectonic disturbance (Fig. 8K). The longest AMS axis k1 has a direction of 220° and a dip of 28.7°. Similar behaviour has been reported on the Paleozoic basement by Chadima et al. (2006) and Grabowski et al. (2009). In this area, the longest AMS axis is produced along the intersection with the sedimentary plane and cleavage, which is caused by movement of the Carpathian nappes, which is in this particular case, the Sub-Silesian unit.

During the Maastrichtian and Paleocene, the opening of flysch basins related to rifting of platforms, olistostromes, and olistoliths were formed in the Silesian Basin by destruction of interbasinal ridges (Cieszkowski et al. 2009). Locally redeposited calcareous algal detritus occurs in this interval (Leszczyński et al. 2012; Waśkowska et al. 2014). The Bystřice section shows both olistostromes (slumps) and algal biodetritic sandstones. The source was probably elevation (ridge) separating the Subsilesian and Silesian part of the Silesian Basin. The K–Pg transition in the Western Carpathians is incomplete in many places due to the effect of Laramian tectonic movements (e. g. Salaj et al. 1978; Soták et al. 2021). Because the Bystřice section seems to be completely Selandian in age and the Maastrichtian sediments seem to be completely redeposited, we cannot speculate about the completeness of the K–Pg transition in this area of the Subsilesian Unit. Regardless, Hanzlíková (1978) reported the *Parvularugoglobigerina eugubina* and *Eoglobigerina fringa* from grey mottled clays of the Subsilesian Unit in the Kateřinice section.

Conclusions

The detailed biostratigraphic study of the Bystřice section proved the Upper Maastrichtian and Selandian age of the sediments, while the Danian is completely absent. Danian strata are known from other parts of the Subsilesian Unit. Rare finds of reworked *Eoglobigerina edita* in the Bystřice section also give evidence for their existence. Stratigraphic repetition in the section is explained by the redeposition of the Maastrichtian sediments by mass flows during the Selandian. The section is strongly remagnetised and the magnetic fabric displays minor tectonic disturbance within the section.

The Maastrichtian original depositional conditions were more reducing and included higher terrestrial plant debris input and slightly higher input of magnetite. Bulk carbonate $\delta^{13}C$ and $\delta^{18}O$ isotopic composition shows more positive values in respect to the Paleocene samples. The presence of Maastrichtian low-latitude calcareous nannofossils indicate the influence of warmer surface waters – a possible warming effect of the Deccan volcanism. The Paleocene proxy parameters suggest a higher share of aquatic (marine) organic matter and oxygenated water column. Paleocene $\delta^{18}O$ isotopes in carbonates show an inverse correlation with $\delta^{13}C$ and more negative values than in the redeposited Maastrichtian sediments.

Acknowledgments: The research was supported by the Czech Science Foundation project no. 19-07516S and is in accordance with research plan no. RVO67985831. The research provides data also for the IGCP 679 project. We are thankful to J. Petráček and K. Bachová for helping with sample preparation and magnetic measurements, as well as P. Pruner for helpful discussions about magnetic results. We thank J. Soták and M. Kędzierski for their helpful reviews.

References

Bown P.R. & Young J.R. 1998: Techniques. In: Bown P.R. (Ed.): Calcareous Nannofossil Biostratigraphy. *British Micropalaeontological Society*, London, 16–28.

Bubík M., Franců J., Gilíková H., Otava J. & Švábenická L. 2016: Upper Cretaceous to Lower Miocene of the Subsilesian Unit (Western Carpathians, Czech Republic): stratotypes of formations revised. *Geologica Carpathica* 67, 239–256. https://doi.org/10.1515/geoca-2016-0016

Burnett J.A. 1998: Upper Cretaceous. In: Bown P.R. (Ed.): Calcareous Nannoplankton Biostratigraphy. *British Micropalaeontological Society*, London, 132–199.

Chadima M. & Hrouda F. 2006: Remasoft 3.0 – a user friendly paleomagnetic data browser and analyser. *Travaux Geophysiques* 27, 20–21.

Chadima M., Hrouda F. & Melichar R. 2006: Magnetic fabric study of the SE Rhenohercynian Zone (Bohemian Massif): Implications for dynamics of the Paleozoic accretionary wedge. *Tectonophysics* 418, 93–109. https://doi.org/10.1016/j.tecto.2005.12.015

Cieszkowski M., Golonka J., Krobicki M., Ślączka A., Oszczypko N., Waśkowska A. & Wendorff M. 2009: The Northern Carpathians plate tectonic evolutionary stages and origin of olistoliths and olistostromes. *Geodinamica Acta* 22, 101–126. https://doi.org/10.3166/ga.22.101-126

Claeys P., Kiessling W. & Alvarez W. 2002: Distribution of Chicxulub ejecta at the Cretaceous–Tertiary boundary. *Geological Society of America Special Papers* 356, 55–68.

Edgar K.M., Wilson P.A., Sexton P.F., Gibbs S.J., Roberts A.P. & Norris R.D. 2010: New biostratigraphic, magnetostratigraphic and isotopic insights into the Middle Eocene Climatic Optimum in low latitudes. *Palaeogeography, Palaeoclimatology, Palaeoecology* 297, 670–682.

Eliáš M. 1998: Sedimentology of the Subsilesian Unit. *Práce Českého geologického ústavu* 8, *Czech Geological Survey*, Prague, 1–48 (in Czech).

Grabowski J., Bábek O., Hladil J., Pruner P., Schnabl P., Werner T., Geršl M. & Otava J. 2009: Late Variscan remagnetization of Devonian carbonates in the Moravo-Silesian zone (Czech Republic): implications for dating tectonic deformation. *Trabajos de Geología* 29, 315–320.

Hanzlíková E. 1978: Biostratigrafie podmenilitového souvrství podslezské jednotky. *Manuscript*, *Archive of the Czech Geological Survey*, Prague, 1–30 (in Czech).

Hanzlíková E. & Švábenická L. 1983: Loc. 20 – Karpentná; profile in the riverbed of Olše. In: Samuel O. & Gašparíková V. (Eds.): 18th European Colloquy on Micropaleontology Excursion-guide. September 11–20, 1983. *Geologický ústav Dionýza Štúra*, Bratislava, 143–145.

Keller G., Punekar J. & Mateo P. 2016: Upheavals during the Late Maastrichtian: Volcanism, climate and faunal events preceding the end-Cretaceous mass extinction. *Palaeogeography, Palaeoclimatology, Palaeoecology* 441, 137–151. https://doi.org/10.1016/j.palaeo.2015.06.034

Kiessling W. & Baron-Szabo R.C. 2004: Extinction and recovery patterns of Scleractinian corals at the Cretaceous–Tertiary boundary. *Palaeogeography, Palaeoclimatology, Palaeoecology* 214, 195−223. https://doi.org/10.1016/j.palaeo.2004.05.025

Killops S. & Killops V. 2004: Introduction to Organic Geochemistry (2nd Edition). *Blackwell Publishing Ltd.*, Oxford, 1−393.

Kirschvink J.L. 1980: The least-squares line and plane and the analysis of paleomagnetic data. *Geophysical Journal of the Royal Astronomical Society* 62, 699–718.

Leszczyński S., Kołodziej B., Bassi D., Malata E. & Gasiński M.A. 2012: Origin and resedimentation of rhodoliths in the Late Paleocene flysch of the Polish Outer Carpathians. *Facies* 58, 367–387. https://doi.org/10.1007/s10347-012-0302-8

Luterbacher H.P., Ali J.R., Brinkhuis H., Gradstein F.M., Hooker J.J., Monechi S., Ogg J.G., Powel J., Röhl U., Sanfilippo A. & Schmitz B. 2004: The Paleogene Period. In: Gradstein F.M., Ogg J.G. & Smith A.G.: A Geologic Time Scale 2004. *Cambridge University Press,* Cambridge, 384–408.

Martini E. 1971: Standard Tertiary and Quaternary calcareous nannoplankton zonation. In: Farinacci A. (Ed.): Proceedings of the Second Planctonic Conference Roma 1970. *Edizioni Tecnoscienza* 2, 739–785.

McCrea J. M. 1950: On the isotopic chemistry of carbonates and a paleotemperature scale. *The Journal of Chemical Physics* 18, 849–857.

Menčík E., Adamová M., Dvořák J., Dudek A., Jetel J., Jurková A., Hanzlíková E., Houša V., Peslová H., Rybářová L., Šmíd B., Šebesta J., Tyráček J. & Vašíček Z. 1983: Geology of Moravskoslezské Beskydy Mts. and Subbeskydian Upland. *Ústřední ústav geologický*, Praha, 1–304 (in Czech).

Olsson R.K., Hemleben Ch., Berggren W.A. & Huber B.T. 1999: Atlas of Paleocene Planktonic Foraminifera *Smithsonian Contributions to Paleobiology* 85, *Smithsonian Institution Press*, Washington DC, 1–252. https://doi.org/10.5479/si.00810266.85.1

Peters K.E., Walters C.C. & Moldowan J.M. 2004: The Biomarker Guide, Volume 1: Biomarkers and Isotopes in the Environment and Human History (2nd edition). *Cambridge University Press*, Cambridge, 1–471. https://doi.org/10.1017/CBO9780511524868

Petersen S.V., Dutton A. & Lohmann K.C. 2016: End-Cretaceous extinction in Antarctica linked to both Deccan volcanism and meteorite impact via climate change. *Nature Communications* 7, 12079, 1–9. https://doi.org/10.1038/ncomms1279

Picha F.J., Stráník Z. & Krejčí O. 2006: Geology and hydrocarbon resources of the Outer Western Carpathians and their foreland, Czech Republic. In: Golonka J. & Picha F.J. (Eds.): The Carpathians and their foreland: Geology and hydrocarbon resources. *AAPG Memoir* 84, 49–175. https://doi.org/10.1306/985607M843067

Salaj J., Kysela J., Gašpariková V. & Began A. 1978: Dán a mont manínskej série západne od Žiliny a otázka laramského vrásnenia. *Geologické Práce, Správy* 70, 57–81 (in Slovak).

Soták J., Elbra T., Pruner P., Antolíková S., Schnabl P., Biroň A., Kdýr Š. & Milovský R. 2021: End-Cretaceous to middle Eocene events from the Alpine Tethys: Multi-proxy data from a reference section at Kršteňany (Western Carpathians). *Palaeogeography, Palaeoclimatology, Palaeoecology* 579, 110571. https://doi.org/10.1016/j.palaeo.2021.110571

Stráník Z. 2021: Flysch Belt. In: Stráník Z., Bubík M., Gilíková H. & Tomanová Petrová P. (Eds.): Geology of the Outer Western Carpathians and southwestern margin of the West-European Platform in Czech Republic. *Czech Geological Survey*, Prague, 95–234 (in Czech).

Švábenická L. 2022: Calcareous nannofossils. Upper Cretaceous of the Bohemian Cretaceous Basin and the Outer Western Carpathians. *Czech Geological Survey*, Prague, 1–150.

Thibault N. & Gardin S. 2010: The calcareous nannofossil response to the end-Cretaceous warm event in the Tropical Pacific. *Palaeogeography, Palaeoclimatology, Palaeoecology* 291, 239–352. https://doi.org/10.1016/j.palaeo.2010.02.036

Thibault N. & Husson D. 2016: Climatic fluctuations and sea-surface water circulation patterns at the end of the Cretaceous era: Calcareous nannnofossil evidence. *Palaeogeography, Palaeoclimatology, Palaeoecology* 441, 152–164. https://doi.org/10.1016/j.palaeo.2015.07.049

Varol O. 1998: Palaeogene. In: Bown P. R. (Ed.): Calcareous Nannoplankton Biostratigraphy. *British Micropalaeontological Society*, London, 200–224.

Waśkowska A., Cieszkowski M., Golonka J. & Kowal-Kasprzyk J. 2014: Paleocene sedimentary record of ridge geodynamics in Outer Carpathian basins (Subsilesian Unit). *Geologica Carpathica* 65, 35–54. https://doi.org/10.2478/geoca-2014-0003

Wierzbicki A. & Kędzierski M. 2020: Maastrichtian climate changes – the calcareous nannofossil record from flysch deposits of the Outer Carpathians. *Annales Societatis Geologorum Poloniae* 90, 447–462. https://doi.org/10.14241/asgp.2020.19

Young J.R., Bown P.R. & Lees J.A. (Eds.) 2018a: Nannotax3 website. International Nannoplankton Association. Accessed February 5, 2018. http://ina.tmsoc.org/Nannotax3

Young J.R., Wade B.S. & Huber B.T. (Eds.) 2018b: pforams@mikrotax website. Accessed April 21, 2017. http://www.mikrotax.org/pforams

Zachos J.C., Pagani M., Sloan L., Thomas E. & Billups K. 2001: Trends, rhythms, and aberrations in global climate 65 Ma to present. *Science* 292, 686–693. https://doi.org/10.1126/science.1059412

Zachos J.C., Dickens G.R. & Zeebe R.E. 2008: An early Cenozoic perspective on greenhouse warming and carbon-cycle dynamics. *Nature* 451, 279–283.

Electronic supplementary material is available online:

Supplement S1 at http://geologicacarpathica.com/data/files/supplements/GC-73-6-Bubik_Suppl_S1.xlsx

Supplement S2 at http://geologicacarpathica.com/data/files/supplements/GC-73-6-Bubik_Suppl_S2.xlsx

Supplement S3 at http://geologicacarpathica.com/data/files/supplements/GC-73-6-Bubik_Suppl_S3.xlsx

Appendix

List of nanno- and microfossils mentioned in the text and tables

Calcareous nannofossils

Arkhangelskiella confusa Burnett 1998
Arkhangelskiella maastrichtiensis Burnett 1998
Biscutum melaniae (Górka 1957) Burnett 1997
Braarudosphaera bigelowii bigelowii (Gran and Braarud 1935) Deflandre 1947
Braarudosphaera bigelowii parvula Stradner 1960
Ceratolithoides kamptneri Bramlette and Martini 1964
Chiasmolithus bidens (Bramlette and Sullivan 1961) Hay and Mohler 1967
Coccolithus pelagicus (Wallich 1877) Schiller 1930
Corollithion exiguum Stradner 1961
Corollithion madagaskarensis Perch-Nielsen 1973
Cribrosphaerella daniae Perch-Nielsen 1973
Cribrosphaerella ehrenbergii (Arkhangelsky 1912) Deflandre in Piveteau 1952
Cruciplacolithus tenuis Hay and Mohler in Hay et al. 1960
Cyclagelosphaera alta Perch-Nielsen 1979
Cyclacelosphaera margerelii Noël 1965
Cyclagelosphaera reinhardtii (Perch-Nielsen 1968) Romein 1977
Discoaster mohleri Bukry and Percical 1971
Eiffellithus parallelus Perch-Nielsen 1973
Eiffellithus pospichalii Burnett 1998
Ellipsolithus distichus Bramlette and Sullivan 1961) Wilcoxon 1967
Ericsonia subpertusa Hay and Mohler 1967
Fasciculithus involutus Bramlette and Sullivan 1961
Fasciculithus tympaniformis Hay and Mohler in Hay et al. 1967
Gonilolithus fluckigeri Deflandre 1957
Heliolithus kleinpellii Sullivan 1964
Lithraphidites quadratus Bramlette and Martini 1964
Markalius apertus Perch-Nielsen 1979
Markalius inversus (Deflndre in Deflandre and Fert 1959) Bramlette and Martini 1964
Micula concava (Stradner in Martini and Stradner 1960) Verbeek 1976
Micula cubiformis Forchheimer 1972
Micula murus (Martini 1961) Bukry 1973
Micula prinsii Perch-Nielsen 1979
Micula staurophora (Gardet 1955) Stradner 1963
Neochiastozygus modestus Perch-Nielsen 1971
Neochiastozygus saepes Perch-Nielsen 1971
Neocrepidolithus cohenii (Perch-Nielsen 1968) Perch-Nielsen 1984
Nephrolithus frequens Górka 1957
Prediscosphaera arkhangelskyi (Reinhardt 1965) Perch-Nielsen 1984
Prediscosphaera majungae Perch-Nielsen 1973
Prediscosphaera microrhabdulina Perch-Nielsen 1973
Prediscosphaera stoveri (Perch-Nielsen 1968) Shafik and Stradner 1971
Reinhardtites elkefensis (Perch-Nielsen 1981) Varol 1991
Reinhardtites levis Prins and Sissingh in Sissingh 1977
Sphenolithus anarrhopus Bukry and Bramlette 1964
Sphenolithus moriformis (Brönnimann and Stradner 1960) Bramlette and Wilcoxon 1967
Sphenolithus primus Perch-Nielsen 1971
Staurolithites laffittei Caratini 1963
Toweius occultatus Perch-Nielsen 1971
Toweius pertusus (Sullivan 1965) Romein 1979
Toweius rotundus Perch-Nielsen in Perch-Nielsen et al. 1978
Toweius tovae Perch-Nielsen 1971
Zeugrhabdotus sigmoides (Bramlette and Sullivan 1961) Burnett and Young 1997

Planktonic foraminifera

Abathomphalus mayaroensis (Bolli 1951)
Acarinina nitida (Martina 1943)
Acarinina strabocella (Loeblich and Tappan 1957)
Acarinina subsphaerica Subbotina 1947
Archaeoglobigerina blowi Pessagno 1967
Archaeoglobigerina cretacea (d'Orbigny 1840)
Chiloguembelina crinita (Glaessner 1937)
Chiloguembelina midwayensis (Cushman 1940)
Chiloguembelina morsei (Kline 1943)
Chiloguembelina trinitatensis (Cushman and Renz 1942)
Contusotruncana contusa (Cushman 1926)
Dicarinella canaliculata (Reuss 1854)
Eoglobigerina edita (Subbotina 1953)
Eoglobigerina eobulloides Morozova 1959
Globanomalina chapmani (Parr 1938)
Globanomalina imitata (Subbotina 1953)
Globanomalina pseudomenardii (Bolli 1957)
Globigerinelloides asper (Ehrenberg 1854)
Globigerinelloides multispinus (Lalicker 1948)
Globigerinelloides subcarinatus (Bronnimann 1952)
Globotruncana aegyptiaca Nakkady 1950
Globotruncana arca (Cushman 1926)
Globotruncana laparrenti Brotzen 1936
Globotruncana rosetta (Carsey 1926)
Globotruncana ventricosa (White 1928)
Globotruncanella petaloidea (Gandolfi 1955)
Globotruncanita angulata (Tilev 1951)
Guembelitria cretacea Cushman 1933
Hedbergella planispira (Tappan 1940)
Hedbergella monmouthensis (Olsson 1960)
Muricohedbergella sliteri Huber 1990
Heterohelix globulosa (Ehrenberg 1840)
Heterohelix labellosa (Nederbragt 1991)
Heterohelix navarroensis Loeblich 1951
Igorina albeari (Cushman and Bermudez 1949)
Igorina pusilla (Bolli 1957)
Igorina tadjikistanensis (Bykova 1953)
Laeviheterohelix dentata (Stenestad 1968)
Laeviheterohelix glabrans (Cushman 1938)
Morozovella acutispira (Bolli et Cita 1960)
Morozovella angulata (White 1928)
Morozovella apanthesma (Loeblich et Tappan 1957)
Morozovella praeangulata (Blow 1979)
Parasubbotina varianta (Subbotina 1953)
Planoglobulina carseyae (Plummer 1931)
Planoglobulina brazoensis Martin 1972
Pseudotextularia elegans (Rzehak 1891)
Pseudotextularia nuttalli (Voorwijk 1937)
Racemiguembelina fructicosa (Egger 1900)
Racemiguembelina powelli Smith et Pessagno 1973
Rugoglobigerina hexacamerata Brönnimann 1952
Rugoglobigerina milamensis Smith et Pessagno 1973
Rugoglobigerina pennyi Brönnimann 1952
Rugoglobigerina rugose (Plummer 1927)
Subbotina cancellata Blow 1979
Subbotina patagonica (Todd et Kniker 1952)
Subbotina triangularis (White 1928)
Subbotina triloculinoides (Plummer 1927)
Subbotina velacoensis (Cushman 1925)